Numerical Simulation of Chronic Moisture Graphite Oxidation for MHTGR

Chengqi Wang,[a] Xiaodong Sun,[a] Richard N. Christensen,[b, c] Shanbin Shi[a]

[a]*Department of Nuclear Engineering and Radiological Sciences, University of Michigan, 2355 Bonisteel Blvd, Ann Arbor, MI*
[b] *Nuclear Engineering Program, The Ohio State University, 201 W. 19th Avenue, Columbus, OH*
[c] *College of Engineering, University of Idaho, 1776 Science Center Drive, Idaho Falls, ID*
nukewang@umich.edu, xdsun@umich.edu, shanbins@umich.edu, christensen.3@osu.edu, rchristensen@uidaho.edu

INTRODUCTION

High Temperature Gas-cooled reactors (HTGRs) are attractive due to its inherent safety features and high thermal-to-electric energy conversion efficiency. However, any small quantity of moisture in the primary helium coolant could threaten reactor structural integrity because of its reaction with graphite components. In addition, a large amount of moisture could invade into the reactor core during a steam ingress accident for HTGRs with Rankine power cycle [1]. The study by Sato et al. showed that an 8% burn-off of graphite could reduce its mechanical strength by 50% [2]. Therefore, it is necessary to investigate the moisture-graphite oxidation for future HTGR development.

The moisture-graphite oxidation is a complex phenomenon involving several physical processes, such as fluid flow, heat and mass transfer, chemical reaction, and material structural changes. It is generally agreed the reaction rate can be expressed by a Langmuir-Hinshelwood (LH) equation [3]. Velasquez obtained the reaction parameters for H-451 graphite by fitting his experimental data to the LH equation [4]. Contescu introduced a temperature-dependent moisture reaction order to the traditional LH equation [5]. These kinetic models make it possible to study the moisture-graphite oxidation numerically. In this paper, a multiphysics model that couples all the aforementioned physical phenomena was established using COMSOL Multiphysics for moisture-graphite oxidation simulation. Although H-451 graphite is no longer in commercial production, Velasquez's kinetic model was applied as reaction source in our study because H-451 was the graphite material in the MHTGR design. Operation conditions of MHTGR were adopted in this study and simulations were run for a 36-month service period. The simulation results indicate that most of the graphite oxidation occurs at the bottom 2~3 fuel blocks in the core due to their higher temperatures. However, those graphite blocks should be able to maintain their mechanical strength and integrity because the oxidation only attacks a 2-mm deep surface layer over the 36-month period.

NUMERICAL MODEL

Chemical Reaction Source

The moisture-graphite oxidation is mainly initiated by the primary heterogeneous reaction (C-H_2O Reaction):

$$\mathrm{C}+\mathrm{H_2O} \rightarrow \mathrm{CO}+\mathrm{H_2} \tag{1}$$

Two secondary reactions also exist:

$$\mathrm{CO}+\mathrm{H_2O} \rightarrow \mathrm{CO_2}+\mathrm{H_2} \tag{2}$$

$$\mathrm{C}+\mathrm{CO_2} \rightarrow 2\mathrm{CO}, \tag{3}$$

which were neglected in this study due to their much smaller reaction rate [6]. The reaction rate of the C-H_2O Reaction, in unit of mol/(m^3-s), is given as [5]:

$$R_s = \frac{\rho_c K_1 p_{\mathrm{H_2O}} F_b F_c}{M_c(1 + K_2 p_{\mathrm{H_2}}^{0.75} + K_3 p_{\mathrm{H_2O}})}, \tag{4}$$

where $\rho_c, F_c, M_c,$ and p are the graphite density, catalytic effect factor (which was assumed to be unity in this study), graphite molar mass, and partial pressure of chemical species, respectively. At the initial stage, the pores in the graphite expand as the graphite is consumed in the C-H_2O Reaction. With the progression of the reaction, a maximum reaction rate will be observed and then the reaction rate decreases because the pores start to collapse, which decreases the total reaction surface area. This effect was accounted for by the burn-off factor F_b:

$$F_b = (1 - X)\sqrt{1 - \psi \ln(1 - X)}, \tag{5}$$

where X is the burn-off and ψ is a graphite property parameter, which was assumed to be 50 [7]. The coefficient K_i in Eq. (4) follows the Arrhenius expression:

$$K_j = k_j \exp\left(-E_j / RT\right), \tag{6}$$

where $k_j, E_j, R,$ and T are the frequency factor, activation energy, specific ideal gas constant, and temperature, respectively. The calculation of K_j was given in Ref. [5].

Mass Transfer Model

The mass transfer was solved for the free flow domain and graphite domain, as expressed by Eqs. (7) and (8):

$$\frac{\partial c_j}{\partial t} + \nabla \cdot \left(-D_{\text{j-mixture}} \nabla c_j\right) + \vec{u}_j \cdot \nabla c_j = 0 \tag{7}$$

$$\frac{\partial c_{\mathrm{j}}}{\partial t}+\nabla\cdot\left(-D_{e,\mathrm{j}}\nabla c_{\mathrm{j}}\right)+\vec{u}_{j}\cdot\nabla c_{\mathrm{j}}=\pm R_{s}, \quad (8)$$

where c, D, and $\vec{u}_{j}$ are the molar concentration, diffusivity and velocity, respectively. The bulk volume diffusivity $D_{\text{j-mixture}}$ was calculated using the method suggested in Ref. [8]. The diffusivity in the graphite domain $D_{\text{e,j}}$ was calculated by considering the Knudsen diffusion:

$$D_{e,\mathrm{j}}=\frac{\varepsilon}{\tau}\frac{D_{\text{j-mixture}}\cdot D_{K,\mathrm{j}}}{D_{\text{j-mixture}}+D_{K,\mathrm{j}}} \quad (9)$$

where ε and $D_{K,\mathrm{j}}$ are the graphite porosity and Knudsen diffusivity. The tortuosity τ was assumed to be [9, 10]:

$$\tau=1/\varepsilon \quad (10)$$

The graphite structural parameters changes as the moisture-graphite reaction proceeds. The chemical reaction rate, graphite burn-off, and porosity can be coupled by solving:

$$\frac{\mathrm{d}X}{\mathrm{d}t}=\frac{M_{c}R_{s}}{\rho_{0}} \quad (11)$$

$$\frac{\mathrm{d}\varepsilon}{\mathrm{d}t}=\left(1-\varepsilon_{0}\right)\frac{\mathrm{d}X}{\mathrm{d}t} \quad (12)$$

The initial graphite density ρ_{0} and porosity ε_{0} are assumed to be 1,770 kg/m^3 and 0.2, respectively [6].

Fluid Flow Model

The fluid flow was simulated by using the $k-\varepsilon$ turbulence model. The micro pore structure in the graphite domain leads to a very small gas velocity, therefore the viscous term becomes predominant, which can be described by the Darcy's law [11]:

$$\frac{\partial}{\partial t}\left(\varepsilon\rho\right)+\nabla\cdot\left(\rho\vec{u}\right)=Q_{m} \quad (13)$$

$$\vec{u}=-\frac{\kappa}{\mu\varepsilon}\nabla p, \quad (14)$$

where Q_{m} and μ are the reaction mass source and viscosity, respectively. The gas mixture permeability κ is modeled by [12]:

$$\kappa=\frac{\varepsilon r_{p}^{2}}{8\tau^{2}}\left(1+\frac{\beta_{s}\mu}{r_{p}p}\sqrt{\frac{RT}{M}}\right), \quad (15)$$

where the gas-wall reflection coefficient β_{s} was assumed to be 5 [12]. With the assumption that no new pores are created during the oxidation process [9, 10], the pore mean diameter can be expressed by:

$$r_{p}=r_{p,0}\sqrt{\varepsilon/\varepsilon_{0}}\,. \quad (16)$$

The static pressure of the free flow was taken as boundary condition for the Darcy's law.

Heat Transfer Model

The heat transfer is simulated by:

$$\rho c_{p}\vec{u}\cdot\nabla T+\nabla\cdot\left(-k_{eff}\nabla T\right)=Q+Q_{\mathrm{vd}}, \quad (17)$$

where ρ, c_{p}, Q, and Q_{vd} are gas mixture density, specific heat, fission power, and chemical reaction power, respectively. The effective thermal conductivity of gas mixture/porous graphite k_{eff} is volume averaged.

Simulation Domain and Boundary Conditions

In the prototypic MHTGR design, the reactor core is consisted of graphite blocks that are machined out from H-451 graphite, in which the coolant channels and fuel holes are drilled. A schematic of one coolant channel unit is shown in Fig. 1(a) [13]. To accelerate the COMSOL calculation, the prototypic structure was simplified into a hollow cylinder with the same coolant channel diameter and fluid-to-solid volume ratio, as shown in Fig. 1(b). The three-dimensional (3-D) hollow cylinder was further simplified into a two-dimensional (2-D) model due to the geometrical symmetry, as shown in Fig. 1(c).

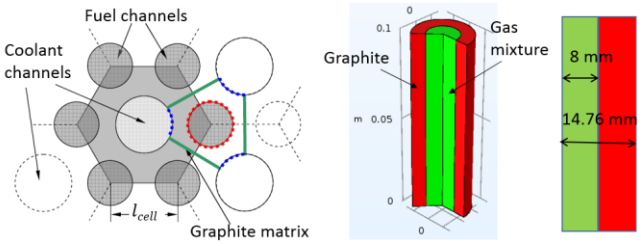

(a) (b) (c)

Fig. 1. Cross-sectional structure of one coolant channel unit in the MHTGR fuel block and simulation domain.

The total length of the simulation domain is 100 mm. The inlet gas mixture (helium, hydrogen, and moisture) is introduced from the top of the domain with a mean velocity of 25 m/s. The moisture-graphite reaction temperature was set by assigning a constant gas mixture inlet temperature. The outlet pressure was assumed to be 6.4 MPa. The thermophysical properties of the gases were extracted from the NIST database [14]. The graphite thermophysical property correlations in Ref. [15] were adopted in this study.

RESULTS AND CONCLUSION

Parametric Studies

According to previous investigations in literature [3-7, 16], the moisture-graphite oxidaition depends on reaction temperature significantly. The reaction transfers from a kinetics controlled regime to a diffusion controlled regime

as reaction temperature increases to exceed a temperature limit. Fig. 2 shows the simulation results of the moistrue concentration in graphite at different reaction temperatures. As can be seen, the moisture concentration in the graphite is almost uniform when the reaction temperature is lower than 925 K. As the temperature increases, the moisture penetration depth into the graphite quickly decreases. When the temperature is higher than about 1,125 K, the moisture can only reach a 2-mm depth surface layer in the graphite. This result matches a conclusion in Ref. [16] that the reaction temperatures lower than 875 K leads to the kinetic regime and the temperatures higher than 1,075 K results in the diffusion controlled regime.

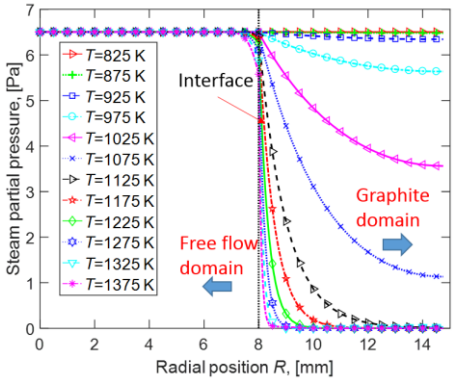

Fig. 2. Effect of reaction temperature on the moisture concentration in graphite ($p_{H_2O} = 6.5\text{Pa}$ in free flow).

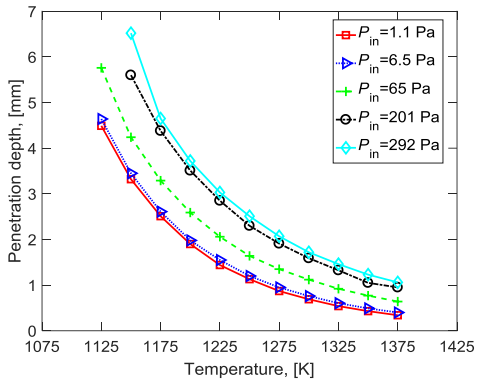

Fig. 3. Effect of reaction temperature and free flow moisture concentration on the moistrue penetration depth.

Simulations were also performed for different free flow moisture concentration levels. To better demonstrate the effects of the reaction temperature and the oxidant partial pressure simultaneously, we define the moisture peneration depth as the distance from the graphite surface to the position at which the steam concentration decreases to 1% of its concentration in the free flow. According to this definition, the penetration depth decreases with the increase of the reaction temperature and moisture concentration in free flow region. However, if the oxidant partial pressure in the free flow is higher than 200 Pa, the effect of the oxidant partial pressure tends to diminish, as shown in Fig. 3.

Longterm Moisture Graphite Oxidation under Normal Operation Conditions

The moisture-graphite oxidation under normal operation conditions was also simulated using the COMSOL model. The sensitivity of oxidation to the fuel block positions was invesitigated by assigning different reaction temperatures. The average block temperature was extracted from Ref. [17], as shown in TABLE I. Six combinations of the moisture and hydrogen concentrations were used in this study, as shown in TABLE II. Hydrogen inhibits oxidation by competing with water moleculars to occupy active graphite sites [5]. Therefore, A3 should exhibite the most severe oxidation among the six cases. The simualtions were run for 36 months.

TABLE I. Fuel Block Temperature [17]

Block No.	Temperature [K]	Block No.	Temperature [K]
1 (top)	623	6	909
2	665	7	991
3	715	8	1,075
4	769	9	1,138
5	831	10 (bottom)	1,164

TABLE II. Combinations of the Moisture and Hydrogen Concentrations

H_2/H_2O concentration	$p_{H_2O} = 1$ Pa	$p_{H_2O} = 5$ Pa	$p_{H_2O} = 15$ Pa
$p_{H_2} = 50$ Pa	A1	A2	A3
$p_{H_2} = 100$ Pa	B1	B2	B3

TABLE III. Graphite Burn-off after 36-Month Operation for Case A3

Block No.	Avg. burn-off (%)	Block No.	Avg. burn-off (%)
1	1.329×10^{-9}	6	2.019×10^{-2}
2	3.748×10^{-8}	7	9.501×10^{-2}
3	1.194×10^{-6}	8	2.310
4	3.007×10^{-5}	9	9.110
5	7.181×10^{-4}	10	16.90

TABLE III shows the burn-off of the 10 blocks at the end of the 36-month service period for Case A3. Only the bottom three blocks were studied in the following analyses because the upper 7 blocks do not exhibit obvious oxidation. The local burn-off distribution is important for reactor structural safety. The graphite burn-off distributions for Cases A2 and A3 are shown in Figs. 4 and 5, respectively. As can be seen, most of the oxidation occurs within a thin layer at the graphite surface. Even at the end of the 36 months, the burn-off at 2 mm depth into the graphite is only ~3 % for the bottom block in Case A2. The burn-off for

Case A3 is much more severe. It should be noted that the condition of A3 is much harsher than the MHTGR design operation conditions while Case A2 represents a more reasonable operation condition. Therefore, it can be concluded that the chronic moisture graphite oxidation results in some surface damage for the bottom three fuel blocks under normal operation conditions. However, the fuel blocks should still maintain its mechanical strength and therefore integrity.

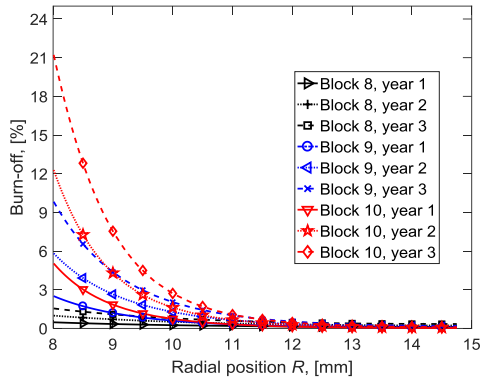

Fig. 4. Graphtie burn-off for Case A2.

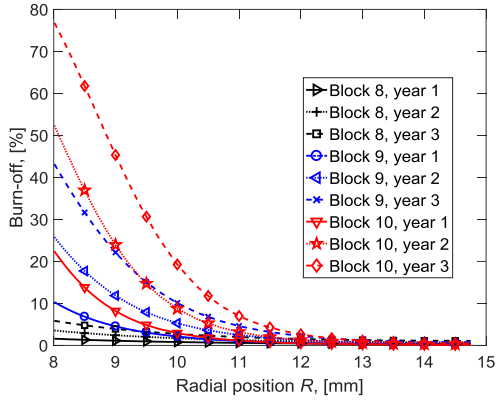

Fig. 5. Graphtie burn-off for Case A3.

Through the above efforts, a multiphysics model has been established and applied for moisture-graphite oxidation studies. This model is able to estimate the oxidation rate, local burn-off and porosity under the normal operation conditions. This model will be used as a start point to evaluate other graphites' performance during normal and/or accidental conditions in the near future.

ACKNOWLEDGMENT

This research was performed using funding received from the U.S. Department of Energy Office of Nuclear Energy's Nuclear Energy University Programs. We also appreciate the insightful comments and valuable suggestions from Dr. Cristian Contescu of the Oak Ridge National Laboratory.

REFERENCES

1. C. WANG, S. SHI, D.J. ARCILESI, X. SUN, and R.N. CHRISTENSEN, "Scaling Analysis and Test Facility Design for Steam Ingress Accident in MHTGR," *Proc. NUTHOS -11*, Gyeongju, Korea, October 9-13, 2000.
2. S. SATO, K. HIRAKAWA, A. KURUMADA, S. KIMURA, and E. YASUD, "Degradation of Fracture Mechanics Properties of Reactor Graphite Due to Burn-off," *Nucl. Eng. Des.*, **118**, 227-241 (1990).
3. P.L. WALKER, F. RUSINKO, and L.G. AUSTIN, "Gas Reactions of Carbon," *Adv. Catal.*, **11**, 133-221 (1959).
4. C. VELASQUEZ, G. HIGHTOWER, and R. BURNETTE, "Oxidation of H-451 Graphite by Steam. Part I. Reaction Kinetics," No. GA-A—14951, General Atomic Co. (1978).
5. C.I. CONTESCU, R.W. MEE, P. WANG, A.V. ROMANOVA, and T.D. BURCHELL, "Oxidation of PCEA Nuclear Graphite by Low Water Concentrations in Helium," *J. Nucl. Mater.*, **453**, 225-232 (2014).
6. M. STEMPHIEWICZ, "Correlation for Steam-graphite Reaction," *Nucl. Eng. Des.*, **280,** 285-293 (2017).
7. X. Yu, L. BRISSONNEAU, C. BOURDELOIE, and S. YU, "The Modeling of Graphite Oxidation Behavior for HTGR Fuel Coolant Channels under Normal Operating Conditions," *Nucl. Eng. Des.*, **238**, 2230-2238 (2008).
8. J.R. WELTY, C.E. WICKS, G. RORRER, and R.E. WILSON, *Fundamentals of Momentum, Heat, and Mass Transfer*, p. 398, John Wiley & Sons, Hoboken, New Jersey (2009).
9. S.K. BHATIA, and D.D. PERLMUTTER, "A Random Pore Model for Fluid-solid Reactions: I. Isothermal, Kinetic Control," *AIChE Journal*, **26**, 379-386 (1980).
10. S.K. BHATIA, and D.D. PERLMUTTER, "A Random Pore Model for Fluid-solid Ractions: II. Diffusion and Transport Effects," *AIChE Journal*, **27**, 247-254 (1981).
11. P.C. CARMEN, *Flow of Gases through Porous Media*, Academic Press, (1956).
12. M.P., BACOS, J.M. DORVAUS, O. LAVIGNE, and Y. RENOLLET, "C/C Composite Oxidation Model: I. Morphological Experimental Investigations," *Carbon*, **38**, 77-92 (2000).
13. R. STAINSBY, et. al., "Investigation of Local Heat Transfer Phenomenon in a Prismatic Modular Reactor Core," NR001/RP/001 R02, AMEC, (2009).
14. NIST, http://webbook.nist.gov/chemistry/
15. J. ORTENSI, et. al. "OECD Benchmark for Prismatic Coupled Neutronics/Thermal Fluids Transient of the MHTGR-350 MW Core Design (Draft)," Idaho National Laboratory (2013).
16. X. LUO, J. ROBIN, and S. YU, "Effect of Temperature on Graphite Oxidation Behavior," *Nucl. Eng. Des.*, **238**, 273-280 (2004).
17. G. STYDOM, and A.S. EPINEY, "Relap5-3D Results for Phase I (Exercise 2) of the OECD/NEA MHTGR-350 MW Benchmark" No. INL/CON-12-24604, Idaho National Laboratory, (2012).